Journal of Membrane Science 325 (2008) 166–175

Contents lists available at ScienceDirect

Journal of Membrane Science

journal homepage: www.elsevier.com/locate/memsci

Preparation of thin-film-composite polyamide membranes for desalination using novel hydrophilic surface modifying macromolecules

Belal J. Abu Tarboush[a], D. Rana[a], T. Matsuura[a,*], H.A. Arafat[b], R.M. Narbaitz[c]

[a] Industrial Membrane Research Laboratory, Department of Chemical and Biological Engineering, University of Ottawa, 161 Louis Pasteur St., Ottawa, ON K1N 6N5, Canada
[b] Department of Chemical Engineering, An-Najah National University, Nablus, West Bank, Palestinian National Authority
[c] Department of Civil Engineering, University of Ottawa, 161 Louis Pasteur St., Ottawa, ON K1N 6N5, Canada

ARTICLE INFO

Article history:
Received 8 April 2008
Received in revised form 7 July 2008
Accepted 10 July 2008
Available online 29 July 2008

Keywords:
Thin-film-composite
Reverse osmosis
Surface modifying macromolecules
Fouling
Desalination

ABSTRACT

A new concept for the preparation of thin-film-composite (TFC) reverse osmosis (RO) membrane by interfacial polymerization on porous polysulfone (PS) support using novel additives is reported. Hydrophi*l*ic *s*urface *m*odifying *m*acromolecules (LSMM) were synthesized both ex situ by *c*onventional method (cLSMM), and *i*n situ within the organic solvent of the TFC system (iLSMM). The effects of these LSMMs on the fouling of the TFC RO membranes used in the desalination processes were studied. FTIR results indicated that both cLSMM and iLSMM were present in the active layer of the TFC membranes. SEM micrographs depicted that heterogeneity of the surface increases for TFC membranes compared to the control PS membrane, and that higher concentrations of LSMM provided smoother surface. AFM characteristic data presented that the surface roughness of the skin surface increases for TFC membranes compared to the control. The RO performance results showed that the addition of the cLSMM significantly decreased the salt rejection of the membrane and slightly reduced the flux, while in the case of the iLSMM, salt rejection was improved but the flux declined at different rates for different iLSMM concentrations. The membrane prepared by the iLSMM exhibited less flux decay over an extended operational period.

1. Introduction

Reverse osmosis (RO) by polymeric membranes is considered as the simplest and most efficient technique for seawater desalination purposes [1]. For the development of these polymeric RO membranes, two different techniques have been used: the phase inversion method for asymmetric membranes, and the interfacial polymerization for thin-film-composite (TFC) membranes [1–3].

TFC membrane preparation technique is based on interfacial polymerization (polycondensation) reaction between two monomers, a polyfunctional amine and a polyfunctional acid chloride, dissolved in water and hydrocarbon solvent, respectively [1–8]. Since water and the hydrocarbon solvent are immiscible, polymerization reaction takes place at the water/hydrocarbon interface. More specifically, the polymerization takes place at the organic phase side of the interface and not the aqueous phase side because of the highly non-favorable partition coefficient for the acid chloride which limits the availability of the acid chloride in the aqueous phase [2,6,9]. The thin film active layer ranging from 10 nm in thickness to several micrometers is quickly formed at the interface and strongly attached to the substrate [10–12]. The art of TFC formation requires selecting the best organic solvent since this parameter governs the amine monomer solubility and diffusivity in the reaction zone, which in fact affect the performance and morphology of the membrane [13]. Recently, Ghosh et al. found that the best TFC performance can be achieved by using high surface tension, and low viscosity solvents [13].

FT-30 membranes, developed by Filmtec Corporation, were of commercial success for RO. In the FT-30, the thin film active layer is aromatic polyamide (PA) that is prepared via interfacial polymerization of *m*-phenylenediamine (MPD) in the aqueous phase and trimesoyl chloride (TMC) in the organic phase [14–16]. FT-30 membranes commercially produced in spiral-wound gives 99.3% salt rejection at 24 gfd flux in seawater desalination at 800 psi [2].

Many attempts have been made to improve the TFC membrane performance through membrane modification or addition of different additives. Kuehne et al. increased TFC-RO flux up to 30–70% by soaking the fresh prepared TFC membranes with solutions containing various organic species, including glycerol, sodium lauryl sulfate, and the salt of triethylamine with camphorsulfonic acid [17]. More recently, Jeong et al. doubled the water flux of RO-TFC membranes without affecting the salt rejection using zeolite nanoparticles in preparing mixed matrix RO-TFC membranes [18].

---

* Corresponding author. Tel.: +1 613 562 5800x6114; fax: +1 613 562 5172.
E-mail addresses: matsuura@eng.uottawa.ca, takeshi_mtsr@yahoo.ca
(T. Matsuura).

0376-7388/$ – see front matter © 2008 Elsevier B.V. All rights reserved.
doi:10.1016/j.memsci.2008.07.037

Additionally, an aqueous solution composed of poly(vinyl alcohol), PVA, and a buffer solution was applied as a post-treatment step during the preparation of the TFC membranes to improve TFC physical properties (improved abrasion resistance) and enhance flux stability [19,20]. On the other hand, high flux TFC membrane at low pressure can be produced by using PVA-based amine compound having a side chain amino group as the aqueous phase monomer instead of the MPD [21].

Despite the high quality of the water produced by TFC-RO process, TFC membranes are susceptible to fouling [22–24]. Fouling, which is defined as the accumulation of substances on the membrane surface or within the membrane pore structure [23–25], always worsens the membrane performance, shortens its life [23], and reduces the flux and salt rejection [26]. In RO membrane desalination, fouling is caused by the interaction between the membrane surface and solute particles and depends strongly on membrane surface morphology [22,26] and properties [27]. RO fouling includes; salt precipitation (i.e., scaling), colloidal fouling, organic fouling, and biofouling [26–33]. Biofouling is considered as the most serious problem since biofouling cannot be prevented using pre-treatment [34,35]. Subramani and Hoek [36] found that the higher the permeate flux, membrane resistance, salt rejection, concentration polarization, membrane hydrophobicity, and membrane surface roughness the higher the microbial cell deposition rates will result.

Many routes were examined to mitigate fouling problem including pre-treatment of the feed solution, modification of membrane surface properties, and periodic cleaning [29,30,37–39]. Meanwhile, surface modification was considered as the most interesting way to prepare fouling-resistant membranes by changing surface-foulant affinity (hydrophilicity or hydrophobicity) or surface morphology [45]. Membrane surface modification can be achieved through grafting, coating [39–44], and blending hydrophilic/hydrophobic *s*urface *m*odifying *m*acromolecules, SMMs [45]. A new type of anti-fouling membranes was developed by introduction of TiO_2 nanoparticles on the TFC membranes. It was demonstrated that this method had the ability to prevent the microbial fouling by reducing the loss of RO permeability [29,38].

Surface hydrophobicity is considered as one of the major reasons of membrane fouling. It is generally accepted that fouling of polymeric membranes decreases with the increase in hydrophilicity of the polymeric materials. It was proposed in many papers that grafting of the surface of the membrane can reduce the fouling [27]. Many hydrophilic monomers have been used for surface modification by grafting such as; poly(ethylene oxide) (PEO), and poly(ethylene glycol) (PEG). PEG, which is a hydrophilic, uncharged, highly water-soluble, and flexible long chain polymer, is well known for its exceptional ability to resist protein adsorption [46,47]. This property is believed to be due to PEG hydrophilicity, large excluded volume, and unique coordination with surrounding water molecules in an aqueous medium [39,48]. Because of its excellent ability to reduce hydrophobic interactions and to repel solutes like proteins, PEG was widely used in preparing fouling-resistant membranes [48,49]. Thom et al. [44] used PEG derivative to produce hydrophilic PSF-UF membranes with high resistance to bovine serum albumin (BSA) fouling. Kang et al. grafted PEG chains onto the surface of TFC-RO membranes to improve membranes resistance to fouling [39].

Introduction of an active additive is considered as another alternative and is a less common approach for surface modification. This method is based on the idea that those additives can move toward the top film surface during membrane formation and alter membrane surface chemistry while keeping bulk properties unchanged [50,51]. Blending is a conventional technique used for membrane surface modification, and recently much attention has been given to utilize this technique with hydrophilic/hydrophobic SMMs blended with the base polymer for membrane surface modification [45,52–55]. Rana et al. used hydrophilic SMM in producing hydrophilic poly(ether sulfone)–ultrafiltration (UF) membranes with high fouling resistance [52].

Surface roughness, is another important factor that affects membrane fouling. In fact, there is a strong relationship between membrane performance (flux, rejection, permeability), and surface structure and morphology [56,57]. Hirose et al. [56] and Kwak et al. [57,58] found that the rougher the surface of the PA-TFC membranes the larger the skin area, and the higher the water flux of the membrane. Preparation of the aromatic PA in the presence of alcohols, ethers, sulfur-containing compounds, and monohydric aromatic compounds and more specifically dimethyl sulfoxide (DMSO) in the aqueous phase can produce membranes with excellent water flux and reasonable salt rejection [15,59–61]. On the other hand, Elimelech et al. found that commercial TFC membrane was fouled faster than cellulose acetate membrane because of the greater surface roughness of the TFC membrane [62].

Based on the extensive analysis above, a novel method is proposed to modify TFC-RO membrane surface. The idea is to incorporate the hydrophi*l*ic SMMs (LSMMs) with PEG end groups to the active polyamide layer in order to render the TFC membrane surface more hydrophilic. In this way, TFC membranes of high fouling resistance can be prepared. The objective of this research is to test the feasibility of this technique.

2. Experimental

2.1. Materials

All chemicals used in this work are listed in Table 1. The chemicals, 4,4′-methylene bis(phenyl isocyanate) (4,4′-diphenylmethane diisocyanate, MDI), 1,3,5-benzenetricarbonyl trichloride (trimesoyl chloride, TMC), 1,4-phenylenediamine (*p*-phenylenediamine, PPD), 1,3-phenylenediamine (*m*-phenylenediamine, MPD), were used without further purification. Commercial UF polysulfone (PS) membranes of molecular weight cut-off (MWCO) 500 kD used as the support membrane were obtained from the TriSep Corporation, Goleta, CA, USA.

2.2. Synthesis of cLSMM, iLSMM and TFC membrane preparation

The *c*onventional hydrophi*l*ic *s*urface *m*odifying *m*acromolecule (cLSMM), end-capped with poly(ethylene glycol), PEG, was synthesized using a two-step solution polymerization method. The initial step involved the reaction of MDI with poly(propylene glycol), PPG, in a common solvent of DMAc. This mixture formed a urethane prepolymer solution. The prepolymer is a segment-blocked urethane oligomer, poly(4,4′-diphenylenemethylene propylene-urethane) having both ends capped with isocyanate. The reaction was then terminated by the addition of PEG resulting in a solution of cLSMM. The chemical structure of the cLSMM is presented in Fig. 1.

The initial reaction step was: 0.02 mol (70 gm) of degassed PPG of average molecular weight 3500 Da in 100 mL of degassed DMAc was added drop-wise to 0.03 mol (7.5 gm) of MDI in 50 mL of degassed DMAc in a 1 L Pyrex round bottom flask with a stirrer. PPG and MDI were allowed to react for 3 h. Then 0.02 mol (20 gm of PEG of average molecular weight 1000 Da) dissolved in 50 mL of degassed DMAc was added drop-wise. The molar mixing ratio of the chemicals MDI:PPG:PEG is 3:2:2. The solution was left under stirring for 24 h at 48–50 °C, resulting in a solution of cLSMM, and then the solution was precipitated in distilled water. The cLSMM was dried in an air circulation oven at 50 °C

Table 1
The materials used in this work

Material description	CAS number	Source
Deuterated *N*,*N*-dimethylformamide (DMF-d_7 99.5 atom% D)	4472-41-7	CDN Isotopes, Point-Claire, PQ, Canada
1,3,5-Benzenetricarbonyl trichloride (TMC)	4422-95-1	Sigma–Aldrich Inc., St. Louis, MO, USA
p-Phenylenediamine (PPD)	106-50-3	Sigma–Aldrich Inc., St. Louis, MO, USA
1,3-Phenylenediamine (MPD, Flakes, 99+%)	108-45-2	Sigma–Aldrich Inc., St. Louis, MO, USA
Octyl acetate, 99+%	112-14-1	Sigma–Aldrich Inc., St. Louis, MO, USA
n-Propyl acetate	109-60-4	BDH Limited, Poole, England
Hexyl acetate, 99+%	142-92-7	Sigma–Aldrich Inc., St. Louis, MO, USA
Nonyl acetate, 97+%, FCC	143-13-5	SAFC Supply Solutions, St. Louis, MO, USA
Heptyl acetate, 98+%	112-06-1	SAFC Supply Solutions, St. Louis, MO, USA
Cyclohexane, 99.9+%	110-82-7	Aldrich Chemicals Co. Inc., Milwaukee, WI, USA
n-Hexane, >+99%	110-54-3	Sigma–Aldrich Inc., St. Louis, MO, USA
N,*N*-Dimethylacetamide (DMAc, anhydrous 99.8%)	127-19-5	Aldrich Chemical Company Inc., Milwaukee, WI, USA
4,4′-Methylene bis(phenyl isocyanate) (MDI, 98%)	101-68-8	Sigma–Aldrich Inc., St. Louis, MO, USA
Poly(ethylene glycol) (PEG, average molecular weight 200 and 1000 Da)	25322-68-3	Sigma Chemical Company, St. Louis, MO, USA
Poly(propylene glycol) (PPG, typical M_n 3500 Da)	25322-69-4	Aldrich Chemical Company Inc., Milwaukee, WI, USA

for 5 days until a constant weight of approximately 64.8 gm was obtained.

The thin-film-composite membrane preparation technique is based on interfacial polymerization between two monomers, di-amine (2 wt%, MPD or PPD) and tri-acid chloride (0.2 wt% TMC), dissolved in water and in hydrocarbon or ester solvent, respectively. Three sets of experiments were made for membrane preparation: the first set using MPD, the second set using PPD, and the third set using MPD.

In the first set, TFC membranes were formed by dipping the PS support in an aqueous MPD solution for approximately 2 h. The saturated membrane was drained and all the excess di-amine solution was removed by holding the membrane in a vertical position for around 3 min. The saturated membrane was then immersed in the organic solution of TMC, with or without cLSMM, for around 2 min, which resulted in the formation of a thin film of polyamide (PA), hereafter called mPA, since it is based on MPD, on top of the PS support. Then, the resulting composite membranes were heat-cured at 90 °C for around 3 min. The membranes were kept under ambient temperature and after 24 h they were washed with distilled water and finally stored in fresh distilled water at ambient temperature.

In the second set, TFC membranes were formed by the same procedure as the first set except that PPD was used instead of MPD, and that the saturated membrane was then immersed in the organic solution of TMC, without cSMM, for 2 min. The thin PA film

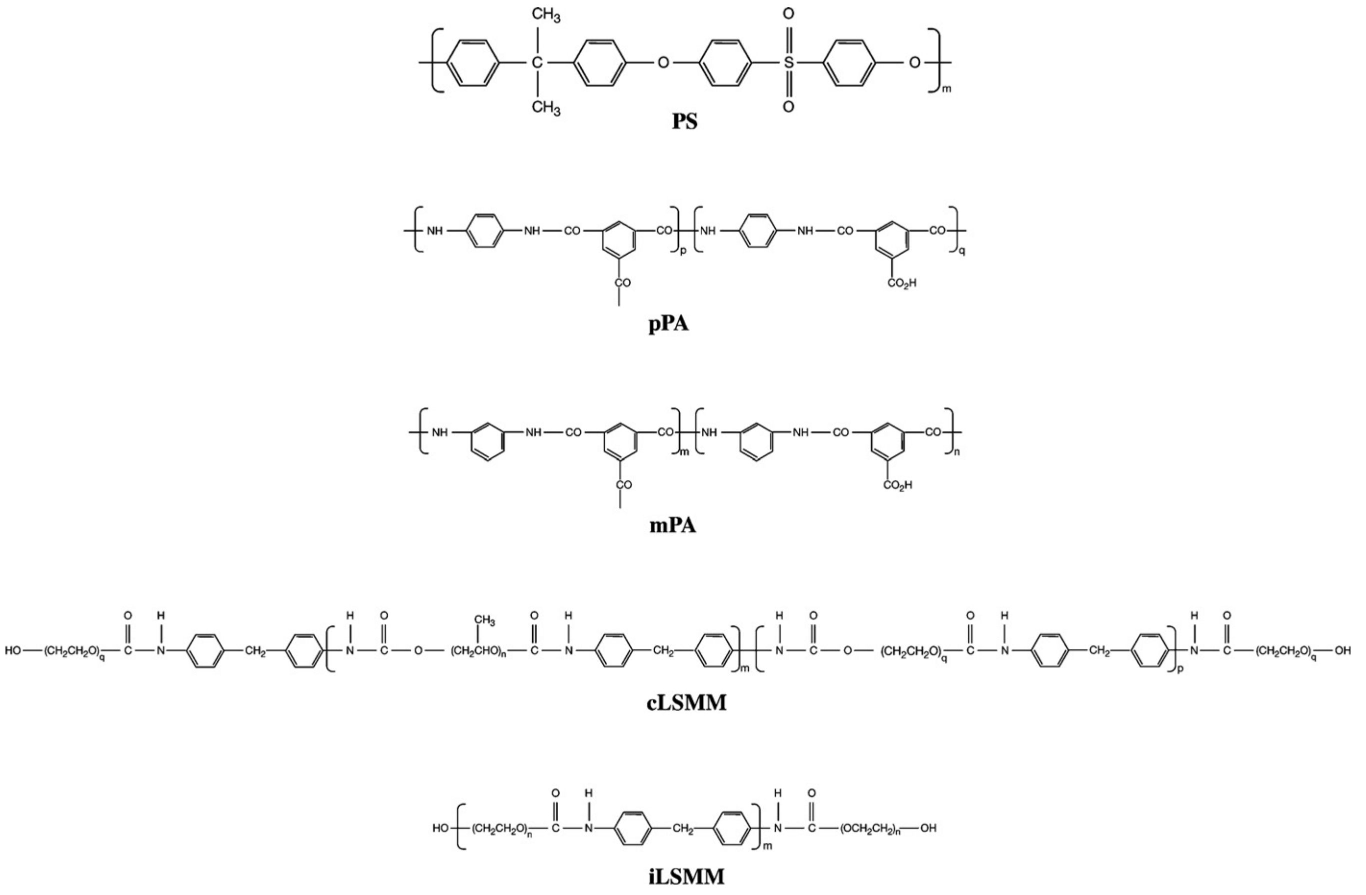

Fig. 1. The chemical structure of polymer materials.

formed on top of the PS support is hereafter called pPA since it is based on PPD. The post-treatment and the storage of the resulting membranes were the same as the first set. In both the first and second sets, *n*-propyl acetate, *n*-hexyl acetate, *n*-octyl acetate, *n*-nonyl acetate, hexane and cyclohexane were tested as solvents for the TMC.

In the third set of TFC membrane formation, MDI and PEG were added to the organic hydrocarbon solvent, cyclohexane, as monomers (di-isocyanate, MDI, and di-ol, PEG) to let the condensation polymerization (LSMM formation) reaction take place in the organic phase parallel to the in situ polymerization (for thin film formation) that was taking place also in the organic phase. The molar ratio of reagents MDI:PEG (average molecular weight 200 Da) was 1:2. The chemical name of the iLSMM is poly(4,4′-diphenylenemethylene ethylene-urethane) with both ends capped by PEG (Fig. 1). The value of the *n* (4.14) was calculated from the average molecular weight of PEG.

The membranes so fabricated are coded as PS-a-b-w, where PS indicates that the support membrane is polysulfone membrane, “a” indicates whether the in situ polymerized thin layer is made of mPA or pPA, “b” indicates whether the LSMM is cLSMM or iLSMM, and “w” indicates the concentration of c(i)LSMM in the organic phase. The concentration of cLSMM is defined as the wt/vol% of cLSMM polymer in the organic solvent, while the concentration of iLSMM is defined as wt/vol% of (MDI + PEG) in the solvent. Thus, membrane code PS means polysulfone support membrane, PS-pPA means polysulfone support membrane coated with a thin film of pPA without any LSMM, and PS-mPA-cLSMM-0.25 means that 0.25 wt% of cLSMM was added to the organic phase.

2.3. Characterization of cLSMM

A sample for NMR analysis was prepared by dissolving as much polymer as possible in DMF-d_7. All NMR data were collected on a Bruker AVANCE 300 NMR spectrometer. The ^{1}H NMR spectra were acquired under quantitative conditions with 16 scans using a 30° pulse, and a 3.6 s interpulse sequence. A ^{1}H–^{13}C heteronuclear single quantum coherence (HSQC) spectrum was collected with 16 scans for each of 256 increments with a 170 ppm ^{13}C spectral window. The data were treated with a shifted sine squared weighting function prior to Fourier transform.

Average molecular weights (weight average molecular weight, M_w, and number average molecular weight, M_n) and polydispersity index (PDI, M_w/M_n) were measured by gel permeation chromatography (GPC) of Waters Associates, Milford, MA. The polymer molecular weights were calculated using the universal calibration curve.

The glass transition temperature (T_g) was examined by differential scanning calorimeter (DSC) (DSC Q1000, TA Instruments, New Castle, DE). The T_g value was recorded of the corresponding heat capacity transition.

2.4. Membrane characterization

The contact angle (CA) of the membrane surface was measured using a VCA Optima Surface Analysis System (AST Products Inc., Billerica, MA). The skin layer surface of membrane was placed on a glass plate, then, a drop of distilled water (2 μL) was placed. The CA was measured at five different spots on each membrane sample coupon and the values averaged.

Fourier transform infrared (FTIR) spectroscopy with attenuated total reflection (ATR) plate was used to observe the presence of functional groups of the membrane. The FTIR spectrometer was (Varian 1000, Varian Inc., Palo Alto, CA, USA). The skin layer of the membrane surface samples was mounted with facing the crystal surface. The spectra were measured in transmittance mode over a wave number range of 4000–600 cm^{-1} at a resolution of 4 cm^{-1}.

The morphology of the membrane was investigated using scanning electron microscopy (SEM) of a model JSM-6400 JEOL (Japan Electron Optics Limited, Japan). Specimen for the SEM of cross-section measurement was prepared by freezing the membrane sample in liquid nitrogen. Fresh cross-sectional cryogenic cut pieces were coated under vacuum with a thin layer (60% gold and 40% palladium) in a Hummer VII sputting system (Anatech, Springfield, VA).

An atomic force microscope (AFM) (Nanosurf AG, Grammetstrasse, Liestal, Switzerland) was used for characterization of membranes. A static force operating mode AFM in air was used. The average surface roughness (R_a) in an area of 1.008×10^{-12} m^2 was obtained for the skin layer of the membrane surface from the software (Nanosurf® easyScan 2, version 1.3) calculation.

2.5. Reverse osmosis experiments

The reverse osmosis (RO) experiments were conducted using a laboratory-scale system consisting of six small RO cells connected in series. The cross-flow cells house membrane coupons with an effective area of about 13.2 cm^2. The feed flow rate was 36 L h^{-1}. The details of the design of the cell and description of the apparatus of RO experiments are given elsewhere [4]. All the experiments were conducted using an operating pressure of 800 psig. Each membrane was pre-compressed by filtering pure water at 1000 psig for 8 h and then for 4–5 h at 800 psig. Pure water permeation (PWP) rates were measured at 800 psig after the pressurization. The sodium chloride concentration in the feed solution was 3.5 wt%. The concentrations of the feed and the permeate solution were determined via a conductivity meter (model CON 110, Oakton Instruments, Vernon Hills, IL, USA).

3. Results and discussion

3.1. Characterization of cLSMM

The ^{1}H, and the HSQC spectrum of cLSMM are shown in Fig. 2a and b, respectively. The presence of the hydroxyl group of the cLSMM sample was confirmed by HSQC spectra in DMF-d_7 solvent as peaks were observed at about 4.7 and 5.1 ppm in the ^{1}H spectra (Fig. 2a) but no signal appeared in the HSQC spectrum (Fig. 2b).

The chemical name of the cLSMM is poly(4,4′-diphenylenemethylene propylene-urethane)-co-poly(4,4′-diphenylenemethylene ethylene-urethane) with both ends capped by PEG. The values of the *n* (60.03) and *q* (22.32) were calculated from the average molecular weight of PPG and of PEG. The values of m and p were calculated using the ^{1}H NMR and M_w of the cLSMM. The ratio between the integrated peak area of the signals corresponding to all hydrogen (AH_T) and the peak area of the methyl signal (AH_M) is expressed as

$$\frac{\sum AH_T}{AH_M} = \frac{6nm + 12m + 12p + 8q + 4pq + 14}{3nm}$$

The right hand side of the equation is formulated from chemical structure of cLSMM (Fig. 1). The left hand side of the equation is equal to 2564.57/1000 from ^{1}H NMR spectra (Fig. 2a). Together with the weight average molecular weight (M_w) data given below, *m* and *p* values were calculated and the results were 3.61 and 17.77, respectively.

The molecular weights characterization data of the cLSMM is $M_n = 1.97 \times 10^4$, $M_w = 3.84 \times 10^4$, PDI = 1.95. The T_g values at the onset and the midpoint of cLSMM are 22.85 and 29.59 °C, respec-

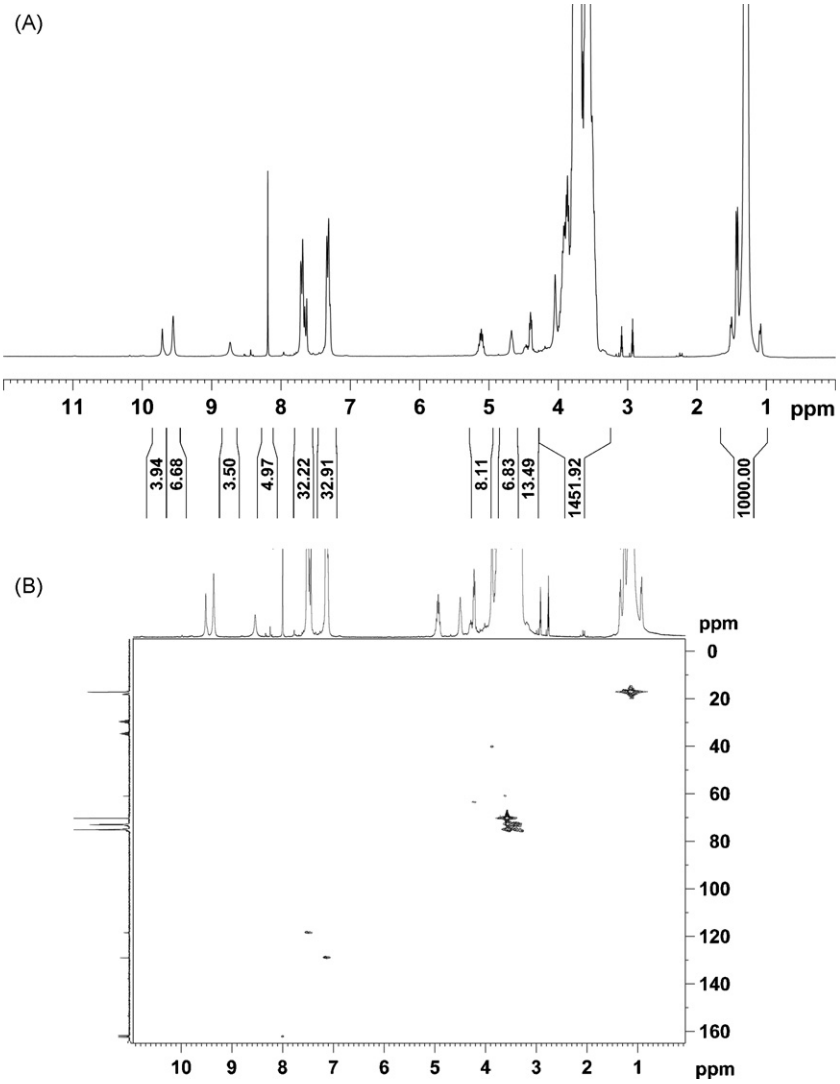

Fig. 2. (A) ^{1}H; (B) HSQC-NMR spectrum of cLSMM.

tively. The molecular weights data indicates that the polymer has low polydispersity while T_g data indicates that the polymer is amorphous and rubbery in nature.

3.2. *Membrane characterization*

The CAs of the membranes are shown in Table 2. TFC membranes with and without addition of LSMM are lower in CA values, and thus are more hydrophilic, than the control PS membrane. According to the table, presence of the thin polyamide layer decreases the CA (CA for PS is 52.8° and for PS-mPA is 31.5°). Upon addition of LSMMs, CA further decreases (CA for PS-mPA-cLSMM-0.25 is 19.8° and for PS-mPA-iLSMM-0.25 is 25.8°). However, increasing the amount of LSMMs to 1 wt% increases the CA value (CA for PS-mPA-cLSMM-1.0 is 29.7° and for PS-mPA-iLSMM-1.0 is 43.9°), indicating a slight increase in hydrophobicity.

Table 2
The contact angle and surface roughness data of the skin layer surface membranes

Membrane	CA (°)	R_a (nm)
PS	52.8 ± 1.9	2.44
PS-mPA	31.5 ± 3.0	9.99
PS-mPA-cLSMM-0.25	19.8 ± 7.3	62.88
PS-mPA-cLSMM-1.00	29.7 ± 4.1	27.97
PS-mPA-iLSMM-0.25	25.8 ± 1.2	55.28
PS-mPA-iLSMM-1.00	43.9 ± 7.3	8.75

The purpose of FTIR spectroscopy is to examine the presence of functional groups present in the skin layer surface of membrane samples. The membranes chosen for the FTIR study are presented in Table 3. The spectra of the base PS membrane shows the peak at 1241.33 and 1150.63 cm^{-1}, assigned to C–O–C and O=S=O, respectively. On the other hand, no PS peaks appeared in the spectrum of the PS-mPA membrane. Instead, peaks appeared at ~3300, 1659.54 and 1609.86 cm^{-1}, which can be assigned to O–H (and N–H), C=O and N–H of mPA. These results confirm the full coverage of the surface by mPA. The presence of carboxylic acid was confirmed by the 1449.86 cm^{-1} peak (see Table 3 for PS-mPA). The presence of cLSMM in the PS-mPA-cLSMM-0.25 and PS-mPA-cLSMM-1.0 membranes was also confirmed by the peaks at 2971.1 and 1103.86 cm^{-1}, which were assigned to C–H of PPG, and C–C–O of PEG and PPG, respectively. Moreover, the intensity of the peak at 2971.10 cm^{-1} increased from 19.51 to 52.43 when the concentration of cSMM in the organic phase was increased from 0.25 to 1.0 wt%. However, the less than fourfold increase in the peak intensity indicates that not all the added cLSMM was incorporated into the mPA skin.

Table 3
The significant peak assignment for FTIR spectra

FTIR peaks (cm^{-1})	Peak assignments
PS membrane	
1585.55, 1487.72	C–C (s)[†] of aromatic
1324.15	C–H of >C(CH_3)
1294.55	O═S═O (s) symmetric
1241.33	C–O–C (s)
1150.63, 1105.83	O═S═O (s) asymmetric
PS-mPA membrane	
~3300	O–H (s) and N–H (s)
1659.54	C═O (b)[‡] of amide
1609.86	N–H (s) of amide
1537.17	C–N (s) of amide
1449.86	C═O (s), O–H (b) of carboxylic acid
PS-mPA-cLSMM membrane (x = 0.25 and 1.00)	
3321.49	O–H (s) and N–H (s)
2971.10	C–H (s) of methyl (PPG)
2868.96	C–H (s) of methylene (PEG, PPG)
1665.10	C═O (b) of amide
1609.86	N–H (s) of amide
1536.65	C–N (s) of amide
1445.29	C═O (s), O–H (b) of carboxylic acid
1103.86	C–C–O of PEG, PPG
PS-mPA-iLSMM membrane (x = 0.25 and 1.00)	
3300.15	O–H (s) and N–H (s)
2874.13	C–H (s) of methylene (PEG)
1722.02	C–O of carboxylic acid
1664.17	C═O (b) of amide
1608.11	N–H (s) of amide
1536.27	C–N (s) of amide
1485.47	C═O (s), O–H (b) of carboxylic acid
1103.69	C–C–O of PEG

[†] s for stretching, [‡] b for bending.

Similarly, the presence of iLSMM was confirmed by the peaks at 2874.13 and 1103.69 cm^{-1}, which are assigned to C–H of PEG, and C–C–O of PEG, respectively. FTIR data support the presence of the hydrophilic amide, hydroxy, and carboxylic acid groups at the membrane surface containing cLSMM and iLSMM which is confirmed by the previous CA data.

The SEM micrographs of the cross-section and the top skin layer of the membranes are presented in Figs. 3–5. The cross-sectional images of the PS membrane and the PS-mPA membrane show that the top surface of the former is very smooth (Figs. 3a and 4a) whereas the top thin film of the composite PS-mPA membrane is rough (Figs. 3b and 4b). Upon addition of LSMM, both PS-mPA-cLSMM and PA-mPA-iLSMM membranes showed a rough surface when the concentration of LSMM in the solvent phase was 0.25 wt% (Fig. 4c and e), while the roughness decreased considerably when the concentration of LSMM was increased to 1 wt% (Fig. 4d and f). Similar images were obtained when the pictures were magnified 10 times at the TFC location of cross-sectional side (Fig. 5). These pictures indicate that the addition of lower concentration (0.25 wt%) of both LSMMs tends to increase the roughness of the thin mPA film. However, the addition of higher concentration (1 wt%) of both LSMMs decreases the surface roughness of the membrane surface. It can be postulated that two phases, one LSMM and the other polyamide, are formed when a small amount of LSMM is added, leading to an increase in surface roughness. However, when a larger amount of LSMM is added the surface is covered by LSMM with a single phase formation, which results in a smoother surface.

The R_a value of the membranes is also cited in Table 2. The R_a value increases from the control PS membrane to the composite PS-mPA membrane due to the thin-film-layer formation over the PS membrane. With addition of lower concentration (0.25 wt%) of LSMM, the R_a increases significantly for both PS-mPA-cLSMM and PS-mPA-iLSMM membranes. With further addition (1.0 wt%) of LSMM, the R_a value tends to decrease. The AFM observation is closely related to the SEM pictures.

3.3. *RO membrane performance*

The effect of organic solvent used for the in situ polymerization on the RO performance was studied for the LSMM-free membranes PS-mPA and PS-pPA as shown in Table 4. From the table, it is quite obvious that PS-mPA (based on MPD) is superior to PS-pPA (based on PPD) in terms of salt rejection for all solvents used. This agrees with the common practice of using MPD, rather than PPD, in the making of RO membranes by most researchers in this field [2,17]. It should be noted that it was extremely difficult to fabricate PS-mPA membranes when esters were used as solvents for the organic phase. Often, white particles were visually noticeable on the membrane surface upon dipping the membrane into the organic phase, indicating a non-uniform PA layer. Nevertheless, TFC membranes could be obtained for *n*-propyl acetate and octyl-acetate and RO data are given for those membranes in Table 4. Membranes could be readily fabricated, on the other hand, with hexane and cyclohexane and the separation data are in the tight nano-filtration (NF) range. In the case of PS-pPA, on the other hand, the separation was poor for most membranes when they were fabricated using esters for the organic phase. In some cases, the top thin film seemed visually detached from the substrate PS membrane. Again, membranes of relatively good performance were obtainable when hexane or cyclohexane was used for the organic phase, although the separation was not as high as PS-mPA membranes.

It is interesting to note that for both PS-mPA and PS-pPA membranes (except for a notable exception of PS-pPA membrane

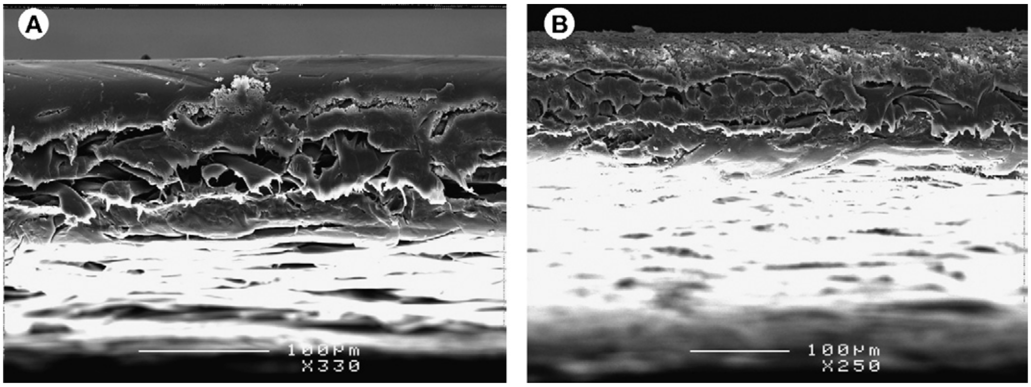

Fig. 3. SEM photographs (100 μm length scale) of the cross-section at surface of the membranes: (A) PS; (B) PS-mPA.

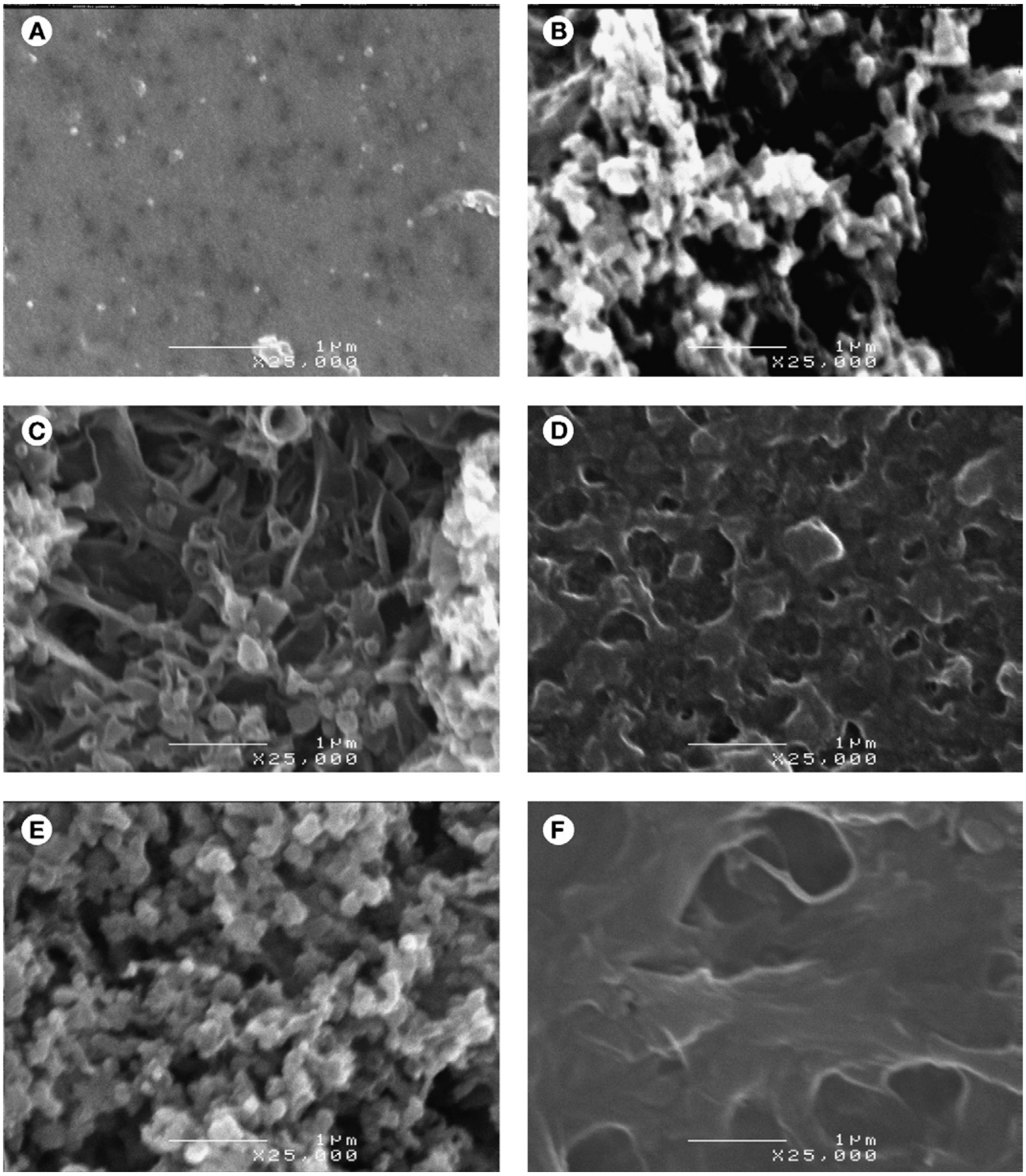

Fig. 4. SEM photographs (1 μm length scale and 25,000× magnification) of the skin layer surface of the membranes: (A) PS; (B) PS-mPA; (C) PS-mPA-cLSMM-0.25; (D) PS-mPA-cLSMM-1.00; (E) PS-mPA-iLSMM-0.25; (F) PS-mPA-iLSMM-1.00.

made with octyl acetate), the separation increased while the flux decreased as the hydrophobicity of the solvent increased as we moved from *n*-propyl acetate to *n*-nonyl acetate and further to hydrocarbons (hexane and cyclohexane). This is probably because the boundary between aqueous and organic phases becomes sharper as the hydrophobicity of organic solvent increases. It is known that hydrophobicity increases as the hydrocarbon chain length of the ester compounds increases and that esters are less hydrophobic than hydrocarbons, including cyclohexane and hexane.

In the next phase of the study, and based on the better performance of PS-mPA compared to PS-pPA, demonstrated so far, PS-mPA membranes with LSMM were studied. In view of the better solubility of cLSMM in cyclohexane than in hexane, the former was chosen for the organic phase to be used thereafter. The effect of LSMM concentration in the organic phase is summarized in Table 5. The table shows that salt rejection decreased significantly upon addition of cLSMM for all cLSMM concentrations. On the other hand, a 50% flux increase, over the control PS-mPA, was observed for the PS-mPA-cSMM-0.05. On the contrary, salt rejection values were considerably higher for membranes with iLSMM than for the PS-mPA, except at the highest iLSMM tested (1 wt%). The best performance with the highest salt sepa-

Table 4
RO performance of various solvents of two different types of TFC coating

Solvent	PWP (L/m^2 h)	Flux (L/m^2 h)	NaCl rejection (%)
PS-mPA membrane			
n-Propyl acetate	106.88 ± 6.42	100.3 ± 1.07	36.4 ± 1.62
Octyl acetate	108.34 ± 3.62	93.1 ± 8.63	50.05 ± 4.45
Hexane	73.87 ± 5.83	30.2 ± 3.25	89.35 ± 2.19
Cyclohexane	75.86 ± 3.465	32.4 ± 3.9	90.2 ± 0.57
PS-pPA membrane			
n-Propyl acetate	215.45 ± 7.70	206.1 ± 8.06	21 ± 1.4
Hexyl acetate	289.6 ± 24.89	181 ± 15.55	16 ± 2.88
Octyl acetate	160.4 ± 54.9	120.2 ± 55.2	38.9 ± 5.09
Nonyl acetate	257.4 ± 7.63	147 ± 7.55	17.9 ± 2.08
Hexane	54.6 ± 2.77	36.4 ± 4.72	77.9 ± 0.90
Cyclohexane	56.7 ± 5.73	37.9 ± 4.93	78.9 ± 2.10

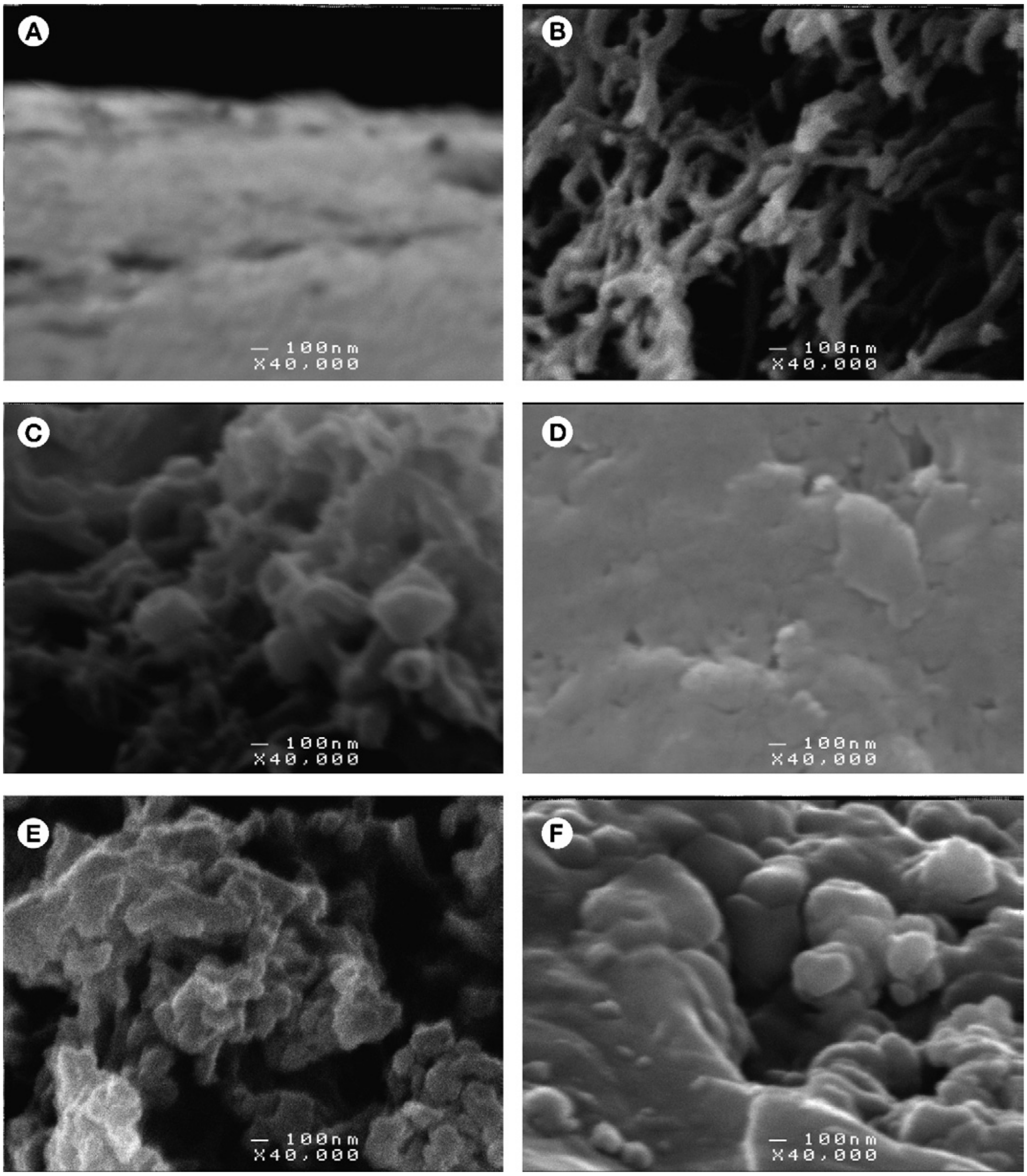

Fig. 5. SEM photographs (100 nm length scale and 40,000× magnification) of the cross-section surface of the membranes: (A) PS; (B) PS-mPA; (C) PS-mPA-cLSMM-0.25; (D) PS-mPA-cLSMM-1.00; (E) PS-mPA-iLSMM-0.25; (F) PS-mPA-iLSMM-1.00.

ration (96.1%) and a reasonably high flux value (24.3 L/m^2 h) was obtained for PS-mPA-iLSMM-0.25 membrane. It is interesting to note that the above membrane exhibited one of the lowest CA values (25.8°) and its surface seemed rougher than other membranes. It should also be noted that addition of a larger amount of iLSMM increased the CA value (43.9° for PS-mPA-iLSMM-1.0 membrane) and the surface became smoother. The membrane performance became poorer, in terms of both salt rejection and flux, correspondingly.

Being the best-performing iLSMM membrane so far, the PS-mPA-iLSMM-0.25 membrane was compared with the LSMM-free PS-mPA for their long-term performance. The results are shown in Fig. 6a for flux and Fig. 6b for salt rejection. The difference in flux data between Table 5 and Fig. 6a reflects the variation of flux data among different membrane coupons, while hardly any difference is noticed between the salt rejection data of Table 5 and those of Fig. 6b. The flux data shown in Fig. 6a clearly indicates the much improved stability of PS-mPA-iLSMM-0.25 membrane as compared to the PS-mPA membrane. It is important to remember that the membranes used here have already been compacted at 1000 psi prior to testing at 800 psi (refer to Section 2), so the observed decline in flux cannot be attributed to membrane compaction. The decline in the flux was only <10% for the PS-mPA-iLSMM-0.25 membrane while it was almost 40% for the PS-mPA membrane during the operational period of 50 h. The improved stability is probably due to the dispersed iLSMM macromolecules in the mPA layer that increases the mechanical strength of the thin mPA layer. The increase in flux stability from PS-mPA membrane to PS-mPA-iLSMM-0.25 membrane is probably due to the presence of PEG groups which has large excluded volume as well as very large coordination number of water molecules at the top surface. The presence of bulky, hydrophilic functional groups at the surface is supported by the low CA value and the rough surface image of this membrane. Fig. 6b indicates that the salt rejection of the PS-mPA-iLSMM-0.25 membrane is much higher than the control PS-mPA membranes. Both membranes remained almost constant in rejection performance throughout the test period.

Table 5
RO performance of various concentrations of two different types of LSMM of TFC coating

	PWP (L/m^2 h)	Flux (L/m^2 h)	NaCl rejection (%)
Concentration of LSMM			
PS-mPA membrane			
0	75.86 ± 3.46	32.40 ± 3.9	90.4 ± 0.76
Concentration of cLSMM			
PS-mPA-cLSMM-*x* membrane (*x* = 0.005–1.00)			
0.005	28.17 ± 0.56	21.77 ± 1.2	66.55 ± 3.32
0.05	50.21 ± 7.0	46.79 ± 14.3	51.5 ± 1.3
0.10	18.56 ± 2.37	15.92 ± 2.68	57.5 ± 2.8
0.30	17.85 ± 7.5	14.95 ± 5.98	65.55 ± 11.6
1.00	12.04 ± 3.27	9.5 ± 3.2	45.7 ± 2.3
Concentration of iLSMM			
PS-mPA-iLSMM-*x* membrane (*x* = 0.10–1.00)			
0.10	52.94 ± 1.94	18.55 ± 1.06	94.3 ± 1.46
0.25	63.93 ± 0.67	24.3 ± 5.20	96.1 ± 2.03
0.50	34.75 ± 7.55	17.9 ± 2.26	91.25 ± 1.48
0.75	11.938 ± 2.42	5.20 ± 0.37	94.2 ± 4.53
1.00	19.93 ± 1.68	9.88 ± 1.93	72.3 ± 7.76

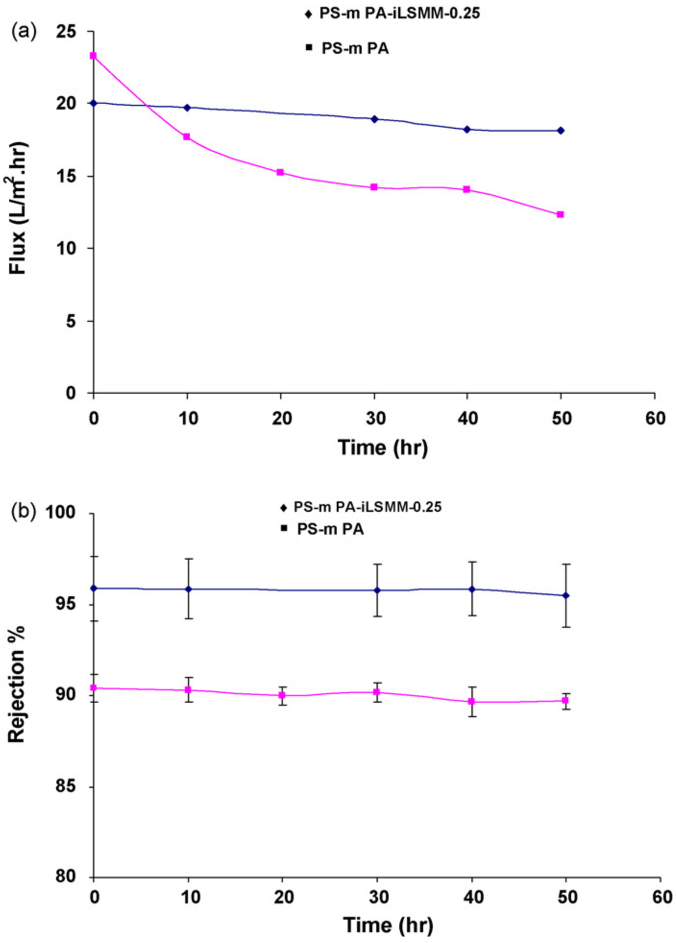

Fig. 6. RO performance (a) flux and (b) separation vs. time.

4. Conclusions

A new concept for the preparation of TFC RO membrane by interfacial polymerization on porous PS support using hydrophilic surface modifying macromolecules (LSMMs) is presented. Those LSMMs are called either cLSMM or iLSMM depending on whether the LSMM is synthesized before (cLSMM) or during (iLSMM) the in situ polymerization. From the experimental results we conclude that both cLSMM and iLSMM could be incorporated in the aromatic polyamide layer of the TFC membrane effectively. The NaCl separation increases while the flux decreases as the hydrophobicity of the solvent is increased in a series of solvents, including either esters or hydrocarbons. The performance of the membrane was better for iLSMM incorporated membrane than cLSMM incorporated membrane. Finally we found that the incorporation of iLSMM increased the stability of membrane desalination performance considerably.

Acknowledgements

This work was supported by the Middle East Desalination Research Center (MEDRC) under project number 05-AS-005. This support is gratefully acknowledged. The authors also gratefully acknowledge the financial support from Natural Sciences and Engineering Research Council of Canada and the Ministry of the Environment, ON, Canada for their partial support of this work.

References

[1] A.P. Rao, N.V. Desai, R. Rangarajan, Interfacially synthesized thin film composite RO membranes for seawater desalination, J. Membr. Sci. 124 (1997) 263.
[2] R.J. Petersen, Composite reverse osmosis and nanofiltration membranes, J. Membr. Sci. 83 (1993) 81.
[3] T. Matsuura, Progress in membrane science and technology for seawater desalination—a review, Desalination 134 (2001) 47.
[4] T. Matsuura, Synthetic Membranes and Membrane Separation Processes, CRC Press, Boca Raton, FL, USA, 1994.
[5] I.J. Roh, J.-J. Kim, S.Y. Park, Mechanical properties and reverse osmosis performance of interfacially polymerized polyamide thin films, J. Membr. Sci. 197 (2002) 199.
[6] V. Freger, Nanoscale heterogeneity of polyamide membranes formed by interfacial polymerization, Langmuir 19 (2003) 4791.
[7] J.E. Cadotte, Reverse osmosis membranes, US Patent 4,259,183 (1981).
[8] L. Li, S. Zhang, X. Zhang, G. Zhang, Polyamide thin film composite membranes prepared from 3,4′,5-biphenyl triacyl chloride 3,3′,5,5′-biphenyl tetraacyl chloride and *m*-phenylenediamine, J. Membr. Sci. 289 (2007) 258.
[9] V. Freger, Kinetics of film formation by interfacial polycondensation, Langmuir 21 (2005) 1884.
[10] S.A. Sundet, Morphology of the rejection surface of aromatic polyamide membranes for desalination, J. Membr. Sci. 76 (1993) 175.
[11] Y. Song, P. Sun, L.L. Henry, B. Sun, Mechanisms of structure and performance controlled thin film composite membrane formation via interfacial polymerization process, J. Membr. Sci. 251 (2005) 67.
[12] V. Freger, S. Srebnik, Mathematical model of charge and density distributions in interfacial polymerization of thin films, J. Appl. Polym. Sci. 88 (2003) 1162.
[13] A.K. Ghosh, B.-H. Jeong, X. Huang, E.M.V. Hoek, Impacts of reaction and curing conditions on polyamide composite reverse osmosis membrane properties, J. Membr. Sci. 311 (2008) 34.
[14] I.J. Roh, A.R. Greenberg, V.P. Khare, Synthesis and characterization of interfacially polymerized polyamide thin films, Desalination 191 (2006) 279.
[15] S.-Y. Kwak, S.G. Jung, S.H. Kim, Structure-motion-performance relationship of flux-enhanced reverse osmosis (RO) membranes composed of aromatic polyamide thin films, Environ. Sci. Technol. 35 (2001) 4334.
[16] Y. Zhou, S. Yu, M. Liu, C. Gao, Polyamide thin film composite membrane prepared from *m*-phenylenediamine and *m*-phenylenediamine-5-sulfonic acid, J. Membr. Sci. 270 (2006) 162.
[17] M.A. Kuehne, R.Q. Song, N.N. Li, R.J. Petersen, Flux enhancement in TFC RO membranes, Environ. Prog. 20 (1) (2001) 23.
[18] B.-H. Jeong, E.M.V. Hoek, Y. Yan, A. Subramani, X. Huang, G. Hurwitz, A.K. Ghosh, A. Jawor, Interfacial polymerization of thin film nanocomposites: a new concept for reverse osmosis membranes, J. Membr. Sci. 294 (2007) 1.
[19] C.N. Tran, A.C. Maldonado, R. Somanathan, Thin-film composite membrane, US Patent 5,234,598 (1993).
[20] C.N. Tran, A.C. Maldonado, R. Somanathan, Method of making thin-film composite membranes, US Patent 5,358,745 (1994).
[21] M. Hirose, Highly permeable composite reverse osmosis membrane and method of producing the same, US Patent 6,837,381 (2005).
[22] M.A. Shannon, P.W. Bohn, M. Elimelech, J.G. Georgiadis, B.J. Mariñas, A.M. Mayes, Science and technology for water purification in the coming decades, Nature 452 (2008) 301.
[23] S. Hong, M. Elimelech, Chemical and physical aspects of natural organic matter (NOM) fouling of nanofiltration membranes, J. Membr. Sci. 132 (1997) 159.
[24] S. Belfer, Y. Purinson, R. Fainshtein, Y. Radchenko, O. Kedem, Surface modification of commercial composite polyamide reverse osmosis membranes, J. Membr. Sci. 139 (1998) 175.

[25] AWWA membrane technology research committee, committee report: membrane processes in portable water treatment, J. AWWA 84 (1) (1992) 59.

[26] X. Zhu, M. Elimelech, Colloidal fouling of reverse osmosis membranes: measurements and fouling mechanisms, Environ. Sci. Technol. 31 (1997) 3654.

[27] S. Belfer, Y. Purinson, O. Kedem, Surface modification of commercial polyamide reverse osmosis membranes by radical grafting: an ATR-FTIR study, Acta Polym. 49 (1998) 574.

[28] W.R. Bowen, T.A. Doneva, H.B. Yin, Atomic force microscopy studies of membrane–solute interactions (fouling), Desalination 146 (2002) 97.

[29] S.H. Kim, S.-Y. Kwak, B. Sohn, T.H. Park, Design of TiO_2 nanoparticles self-assembled aromatic polyamide thin-film-composite (TFC) membrane as an approach to solve biofouling problem, J. Membr. Sci. 211 (2003) 157.

[30] N. Park, B. Kwon, I.S. Kim, J. Cho, Biofouling potential of various NF membranes with respect to bacteria and their soluble microbial products (SMP): characterizations, flux decline, and transport parameters, J. Membr. Sci. 258 (2005) 43.

[31] M. Al-Ahmad, F.A. Abdul Aleem, A. Mutiri, A. Ubaisy, Biofouling in RO membrane systems. Part 1. Fundamentals and control, Desalination 132 (2000) 173.

[32] S.-T. Kang, A. Subramani, E.M.V. Hoek, M.A. Deshusses, M.R. Matsumoto, Direct observation of biofouling in cross-flow microfiltration: mechanisms of deposition and release, J. Membr. Sci. 244 (2004) 151.

[33] S. Kang, E.M.V. Hoek, H. Choi, H. Shin, Effect of membrane surface properties during the fast evaluation of cell attachment, Sep. Sci. Technol. 41 (2006) 1475.

[34] M.F.A. Goosen, S.S. Sablani, H. Al-Hinai, S. Al-Obeidani, R. Al-Belushi, D. Jackson, Fouling of reverse osmosis and ultrafiltration membranes: a critical review, Sep. Sci. Technol. 39 (2005) 2261.

[35] J.S. Baker, L.Y. Dudley, Biofouling in membrane systems—a review, Desalination 118 (1998) 81.

[36] A. Subramani, E.M.V. Hoek, Direct observation of initial microbial deposition onto reverse osmosis and nanofiltration membranes, J. Membr. Sci. 319 (2008) 111.

[37] M. Mulder, Basic Principles of Membrane Technology, second ed., Kluwer Academic Publishers, Dordrecht, The Netherlands, 1991.

[38] S.-Y. Kwak, S.H. Kim, S.S. Kim, Hybrid organic/inorganic reverse osmosis (RO) membrane for bactericidal anti-fouling. 1. Preparation and characterization of TiO_2 nanoparticles self-assembled aromatic polyamide thin-film composite (TFC) membrane, Environ. Sci. Technol. 35 (2001) 2388.

[39] G. Kang, M. Liu, B. Lin, Y. Cao, Q. Yuan, A novel method of surface modification on thin-film composite reverse osmosis membrane by grafting poly(ethylene glycol), Polymer 48 (2007) 1165.

[40] A. Nabe, E. Staude, G. Belfort, Surface modification of polysulfone ultrafiltration membranes and fouling by BSA solutions, J. Membr. Sci. 133 (1997) 57.

[41] B. Kaeselev, J. Pieracci, G. Belfort, Photoinduced grafting of ultrafiltration membranes: comparison of poly(ether sulfone) and polysulfone, J. Membr. Sci. 194 (2001) 245.

[42] D.S. Wavhal, E.R. Fisher, Membrane surface modification by plasma-induced polymerization of acrylamide for improved surface properties and reduced protein fouling, Langmuir 19 (2003) 79.

[43] D.S. Wavhal, E.R. Fisher, Hydrophilic modification of polyethersulfone membranes by low temperature plasma-induced graft polymerization, J. Membr. Sci. 209 (2002) 255.

[44] V. Thom, K. Jankova, M. Ulbricht, J. Kops, G. Jonsson, Synthesis of photoreactive α-4-azidobenzoyl-ω-methoxy poly(ethylene glycol)s and their end-on photografting onto polysulfone ultrafiltration membranes, Macromol. Chem. Phys. 199 (1998) 2723.

[45] D. Rana, T. Matsuura, R.M. Narbaitz, Novel hydrophilic surface modifying macromolecules for polymeric membranes: polyurethane ends capped by hydroxy group, J. Membr. Sci. 282 (2006) 205.

[46] P. Wang, K.L. Tan, E.T. Kang, K.G. Neoh, Synthesis, characterization and anti-fouling properties of poly(ethylene glycol) grafted poly(vinylidene fluoride) copolymer membranes, J. Mater. Chem. 11 (2001) 783.

[47] J. Wang, C.J. Pan, N. Huang, H. Sun, P. Yang, Y.X. Leng, J.Y. Chen, G.J. Wan, P.K. Chu, Surface characterization and blood compatibility of poly(ethylene terephthalate) modified by plasma surface grafting, Surf. Coat. Technol. 196 (2005) 307.

[48] J.H. Lee, H.B. Lee, J.D. Andrades, Blood compatibility of polyethylene oxide surfaces, Prog. Polym. Sci. 20 (1995) 1043.

[49] L. Szleifer, Polymers and proteins: interactions at interfaces, Curr. Opin. Solid State Mater. Sci. 2 (1997) 337.

[50] M. Khayet, D.E. Suk, R.M. Narbaitz, J.P. Santerre, T. Matsuura, Study on surface modification by surface-modifying macromolecules and its applications in membrane separation processes, J. Appl. Polym. Sci. 89 (2003) 2902.

[51] M. Khayet, Membrane surface modification and characterization by X-ray photoelectron spectroscopy, atomic force microscopy and contact angle measurements, Appl. Surf. Sci. 238 (2004) 269.

[52] D. Rana, T. Matsuura, R.M. Narbaitz, C. Feng, Development and characterization of novel hydrophilic surface modifying macromolecule for polymeric membranes, J. Membr. Sci. 249 (2005) 103.

[53] V.A. Pham, J.P. Santerre, T. Matsuura, R.M. Narbaitz, Application of surface modifying macromolecules in polyethersulfone membranes: influence on PES surface chemistry and physical properties, J. Appl. Polym. Sci. 73 (1999) 1363.

[54] L. Zhang, G. Chowdhury, C. Feng, T. Matsuura, R. Narbaitz, Effect of surface-modifying macromolecules and membrane morphology on fouling of polyethersulfone ultrafiltration membranes, J. Appl. Polym. Sci. 88 (2003) 3132.

[55] A. Hamza, V.A. Pham, T. Matsuura, J.P. Santerre, Development of membranes with low surface energy to reduce the fouling in ultrafiltration applications, J. Membr. Sci. 131 (1997) 217.

[56] M. Hirose, H. Ito, Y. Kamiyama, Effect of skin layer surface structures on the flux behavior of RO membranes, J. Membr. Sci. 121 (1996) 209.

[57] S.-Y. Kwak, S. Jung, Y. Yoon, D. Ihm, Details of surface features in Aromatic polyamide reverse osmosis membranes characterized by scanning electron and atomic force microscopy, J. Polym. Sci. Part B: Polym. Phys. 37 (1999) 1429.

[58] S.-Y. Kwak, M. Yeom, I.J. Roh, D.Y. Kim, J. Kim, Correlations of chemical structure, atomic force microscopy (AFM) morphology, and reverse osmosis (RO) characteristics in aromatic polyester high-flux RO membranes, J. Membr. Sci. 132 (1997) 183.

[59] M. Hirose, K. Ikeda, Method of producing high permeable composite reverse osmosis membrane, US Patent 5,576,057 (1996).

[60] M. Hirose, H. Ito, M. Maeda, K. Tanaka, Highly permeable composite reverse osmosis membrane, method of producing the same, and method of using the same, US Patent 5,614,099 (1997).

[61] S.H. Kim, S.-Y. Kwak, T. Suzuki, Positron annihilation spectroscopic evidence to demonstrate the flux-enhancement mechanism in morphology-controlled thin-film-composite (TFC) membrane, Environ. Sci. Technol. 39 (2005) 1764.

[62] M. Elimelech, X. Zhu, A.E. Childress, S. Hong, Role of membrane surface morphology in colloidal fouling of cellulose acetate and composite aromatic polyamide reverse osmosis membranes, J. Membr. Sci. 127 (1997) 101.